Supporting Information

Machine Learning Optimized Bimetallic MOF/MXene Composite with Improved Supercapacitor Performance

Sagheer Ahmad [a], Muhammad Ali Khan [a*], Ameer Hamza [b], Hafiz Muhammad Asif [a], Aqsa [a], Farhan Zafar [c], Muhammad Sohail [a]

[a]Institute of Chemical Sciences, Bahauddin Zakariya University (BZU), Multan 60800, Pakistan

[b]Department of Chemistry, University of Southern California, Los Angeles, USA.

[c]Department of Chemistry, COMSATS University Islamabad, Lahore Campus, Lahore 54000, Pakistan

***Corresponding Author:**

Dr. Muhammad Ali Khan
Email: malikhan@bzu.edu.pk
Tel: +923013419292

Characterization Instrumentation

Instruments used during this scientific work were Fourier transform infrared spectroscopy (FTIR) IRA affinity-1S spectrophotometer-USA to record FTIR spectra of CoZn-ZIF@MXene in the range of 500-4000 cm^{-1}. X-ray diffraction (XRD) was measured by Rigaku, Miniflex-II-Japan by means of Cu Kα (with a scan angle: 5^{o}-80^{o}, at 40 kV, 40 mA, and (2q). The surface morphological analyses of the synthesized materials were analyzed using scanning electron microscopy (SEM) at a Zeiss Evo 50 XVP (Oxford instruments INCA, X.act, S.No. 56756, UK). All the electrochemical investigations were carried out using the Gamry interface (1010E) potentiostate. This potentiostate instrument contains three electrodes such as working electrode, reference electrode and auxiliary electrode.

Machine Learning

Machine learning (ML) algorithms were employed to predict and optimize the specific capacitance of the synthesized electrode materials. The ML was carried out using the Scikit-learn library in Python 3. A range of supervised regression models-including Linear Regression (LR), Ridge Regression (RR), Decision Tree Regression (DTR), Random Forest Regression (RFR), Gradient Boosting Regression (GBR), K-Nearest Neighbor Regression (KNNR), Support Vector Regression (SVR), and Extreme Gradient Boosting Regression (XGBR) were employed to establish quantitative relationships between the experimental input features (e.g., concentrations of Co, Zn, and MXene) and the target output (specific capacitance).

The total dataset comprised 64 experimental data points, which were systematically divided into 38 for training, 13 for validation, and 13 for independent testing, corresponding to approximately 70%, 15%, and 15% of the dataset, respectively. This three-way data splitting strategy ensured unbiased model training, hyperparameter tuning, and performance evaluation. Each model was trained using the training dataset, optimized based on validation performance, and finally assessed on the test dataset to evaluate its generalization capability. The performance of the models was assessed using two standard statistical metrics: the coefficient of determination (R^2), which indicates the proportion of variance in the target variable explained by the model, and the

root mean square error (RMSE), which reflects the average deviation between predicted and actual values.

Among the models tested, the XGBR algorithm exhibited superior performance, achieving the highest R^2 and lowest RMSE values. This indicates that the XGBR model was most effective in capturing the complex nonlinear relationships between the input variables and the specific capacitance. The optimized XGBR model was subsequently employed to identify the optimal concentrations of Co, Zn, and MXene that maximize specific capacitance. This work underscores the novelty of applying a multi-model regression framework to guide materials design for energy storage applications, thereby bridging computational prediction with experimental realization.

Synthesis of ZIF-8@MXene

$Zn(CH_3COO)_2.2H_2O$ (219 mg), was dissolved in 10 mL DI water in a conventional synthesis. After that, this solution was quickly injected into an aqueous solution (70 mL) of MXene containing 4.54 g of 2-MIM, and it was agitated for 20 minutes at room temperature. Then it was centrifuged to get product, washed repeatedly with DI for subsequent use.

Synthesis of ZIF-67@MXene

$Co(NO_3)_2.6H_2O$ (292 mg), was dissolved in 10 mL of DI water that contained 5 mg of CTAB. This solution was quickly added into 70 mL of DI water containing 4.54 g of 2-MIM, and it was agitated for 20 minutes at room temperature. Then it was centrifuged to get product, washed repeatedly with DI for subsequent use.

Fabrication of working electrode

The electrochemical properties of the synthesized materials were determined by using an electrochemical workstation Gamry potentiostate 1010E (electrochemical analyzer). The electrochemical tests like cyclic voltammetry (CV), galvanostatic charge discharge (GCD) and electrochemical impedance spectroscopy (EIS) measurements were performed in the frequency range of 10 kHz to 0.1 Hz with an open circuit voltage. The three-electrode system was used, Ag/AgCl and platinum wire were used as reference and counter electrode respectively. The working electrode was nickel foam with an area of $1cm^{-2}$. The active material was deposited on the working electrode by adding ZIF powder to ethanol after bath sonication for 30 minutes and

it was added dropwise to the nickel foam and dried at room temperature. 1 M KOH solution was used as an electrolyte for the EIS, CV and GCD measurements of all samples.

Mechanism

Two separate oxidation-reduction peaks on the CoZn-ZIF@MXene CV curve can be seen, which represent the redox reaction between the cations in the composite material and the OH^- in the electrolyte solution. The charging and discharging rates have the most influence on the oxidation and reduction peaks, which exhibit modest shifts toward positive and negative potentials as the scan rate rises. The possible electrochemical reactions during energy storage process of CoZn-ZIF@MXene can be seen in the following equations S1 and S2 [1].

$$Co(OH)_2 + OH^- \longleftrightarrow CoOOH + H_2O + e^- \quad (S1)$$

$$Zn(OH)_2 + OH^- \longleftrightarrow ZnOOH + H_2O + e^- \quad (S2)$$

Calculations of Electrochemical Analysis

Specific capacitance was calculated from CV curves using the equation S3 [2].

$$C_s = \frac{A}{m \times k \times \Delta U} F/g \quad \textbf{(S3)}$$

Where *C*s represents the specific capacitance in F/g, A represents area under CV curve, m represents the mass of electroactive material in g, *K* represents the potential scan rate in V/s, and Δ*U* represents the potential window.

Specific capacitance was also calculated from the GCD curves using the equation S4 [2].

$$C_s = \frac{I \times \Delta t}{m \times \Delta U} F/g \quad \textbf{(S4)}$$

Where I/m represents the current density in A/g, Δt represents the discharging time and ΔU represents the voltage window.

Pseudocapacitive contribution calculations

Pseudocapacitance contribution at a specific scanning rate can be seen from the following equations [3] :

$$i(V) = k_1 v + k_2 v^{1/2} \quad \textbf{(S5)}$$

$$\frac{i(V)}{v^{1/2}} = k_1 v^{1/2} + k_2 \quad \textbf{(S6)}$$

Where $k_1 v$ and $k_2 v^{1/2}$ represents the currents governed by capacitive contribution and diffusion contribution respectively. The slope and intercept of the fitted curve can be used to determine the values of k_1 and k_2.

The energy density and power density can be calculated by using equation 7 and 8 [4].

$$E = \frac{0.5 \times Csp \times \Delta V^2}{3.6} \quad (S7)$$

$$P = E \times \frac{3600}{\Delta t} \quad (S8)$$

EDX

The Energy dispersive X-ray spectroscopy (EDX) was studied to analyze elemental composition and elemental abundance based on the X-ray peak intensity. In (Fig. S1D) Titanium (Ti) is represented by a strong peak in the spectrum that is situated in the 4.5–5 keV range. The existence of titanium, the main transition element in the MXene structure, is confirmed by this strong Ti signal. According to the Ti3C2Tx composition, the high intensity of this peak indicates that titanium makes up a significant portion of the material. The EDX spectrum of CoZn-ZIF@MXene (Fig. S1A) shows the presence of cobalt (Co) and zinc (Zn) from the CoZn-ZIF as well as titanium (Ti) from the MXene structure. The MXene layers and the organic ligands in the ZIF structure are correlated with the carbon peak. Potassium is possibly a remnant or contaminant element. This demonstrates that the composite material has all the necessary elements for the multipurpose uses for which it was designed.

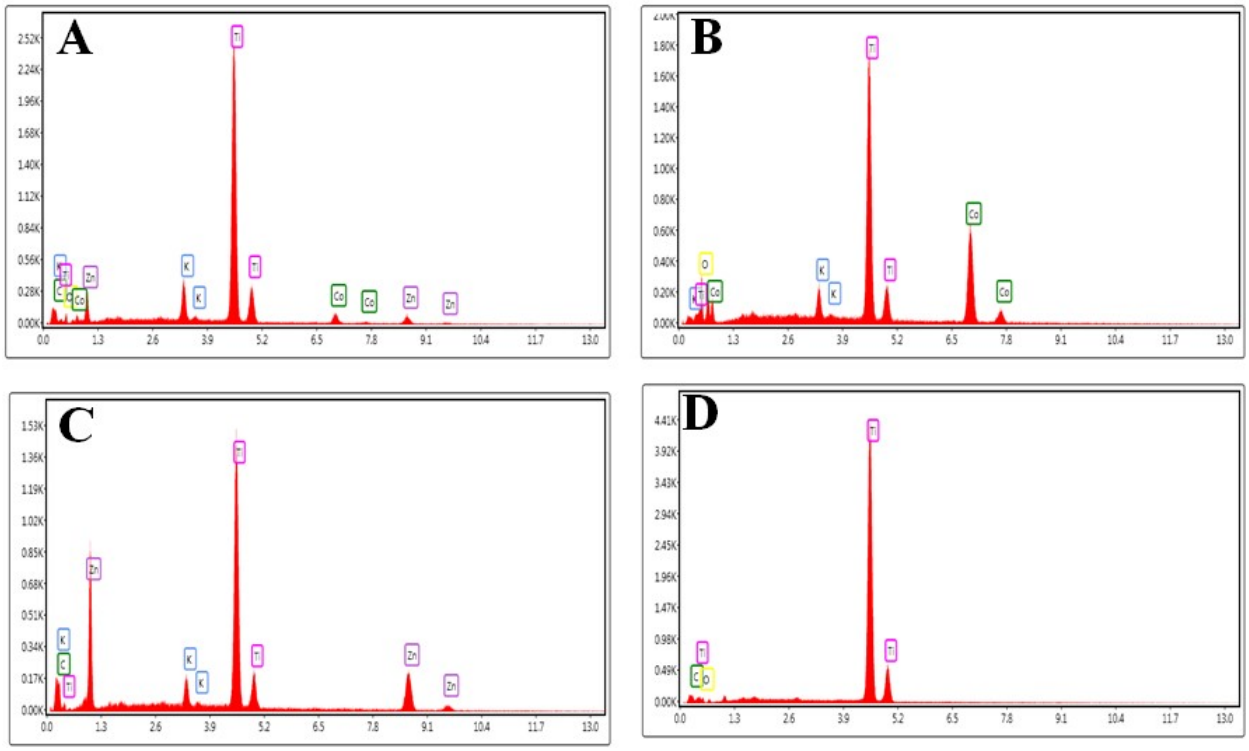

Figure S1. Elemental analysis results from energy dispersive x-ray spectrometer (A) CoZn-ZIF@MXene (B) ZIF-67@MXene (C) ZIF-8@MXene (D) MXene.

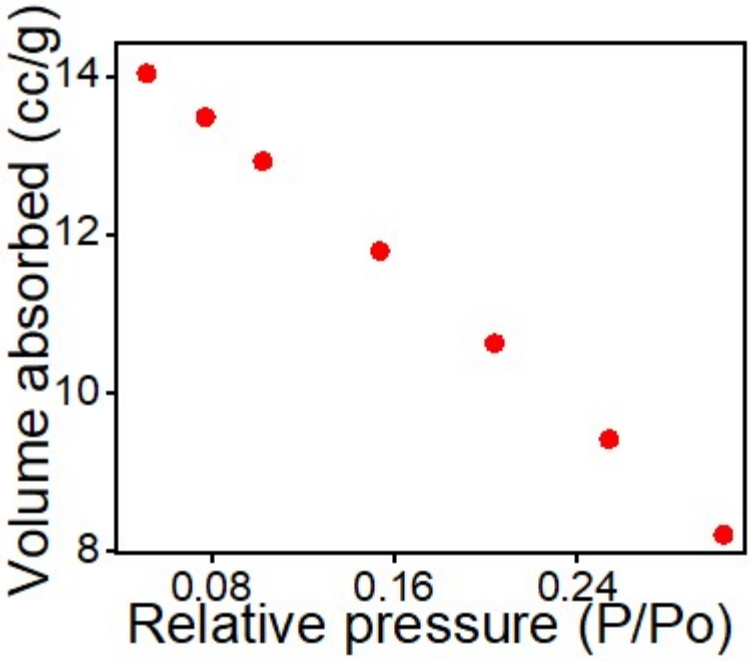

Figure S2. Show multi-point BET of CoZn-ZIF@MXene.

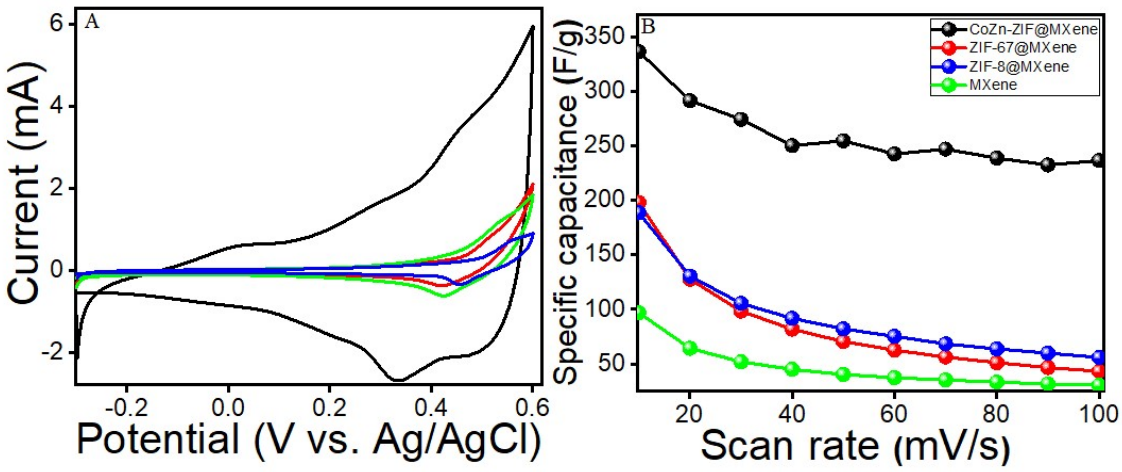

Figure S3. shows (A) Comparative CV (B) Specific capacitance as a function of scan rate.

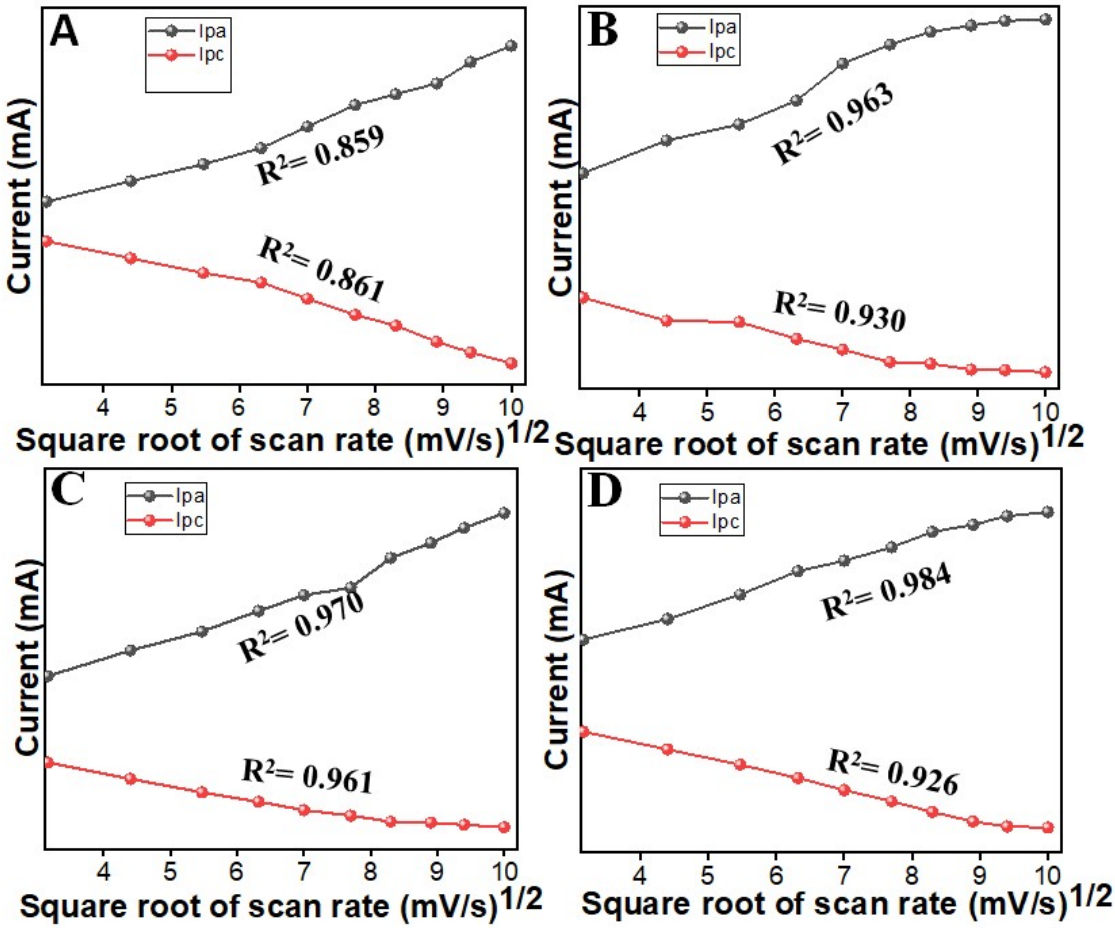

Figure S4. Plot of anodic and cathodic peak current versus square root of scan rate for (A) CoZn-ZIF@MXene, (B) ZIF-67@MXene, (C) ZIF-8@MXene, and (D) MXene.

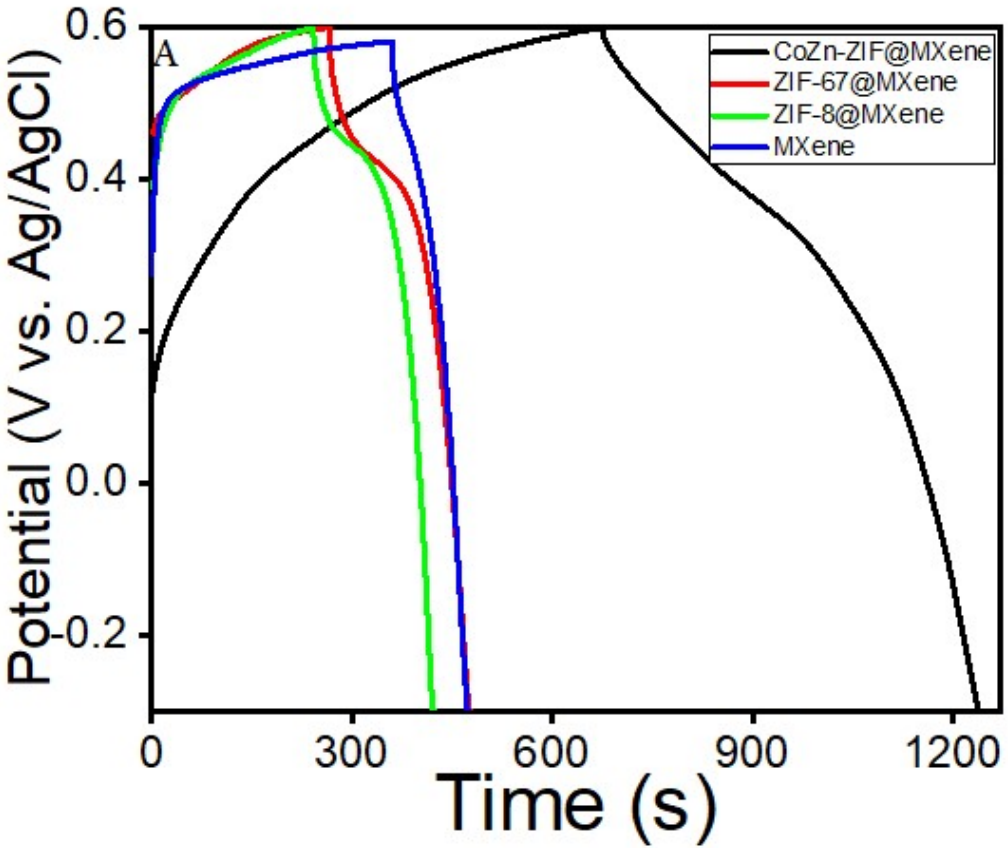

Figure S5. Comparative GCD graphs for different electrodes at current density of 3 A/g.

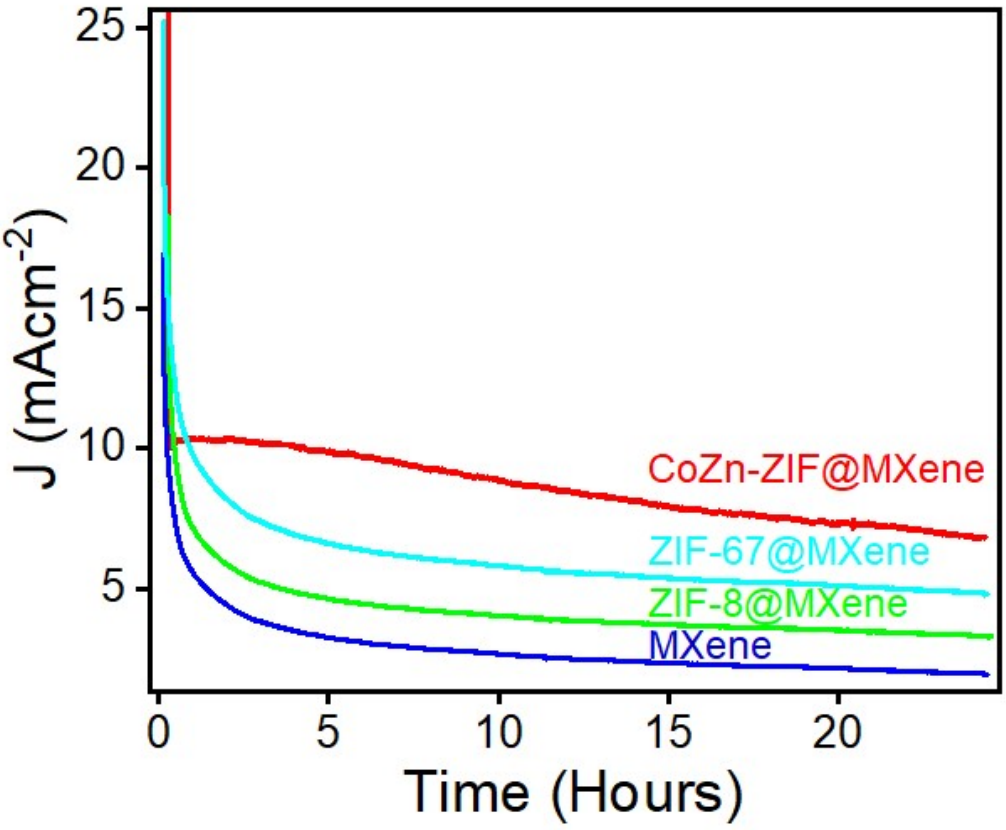

Figure S6. Shows chronoamperometric measurements to test the durability of CoZn-ZIF@MXene, ZIF-67@MXene, ZIF-8@MXene, and MXene.

Table S1. Shows performance comparison of various machine learning models for predicting overpotential, showcasing Train RMSE, Validation RMSE, Test RMSE, and R^2 scores.

Model	Train RMSE	Validation RMSE	Test RMSE	R^2 Score
Linear Regression	1.89	1.17	2.56	0.57
Ridge Regression	2.84	2.97	3.20	0.33
Decision Tree Regression	0.00	1.03	0.77	0.96
Random Forest Regression	0.45	0.87	1.13	0.92
Gradient Boosting Regression	0.19	0.91	0.65	0.97
K-nearest neighbor Regression	1.58	2.34	2.25	0.67

Support Vector Regression	1.84	2.51	2.47	0.61
XGBoost Regression	0.00	1.25	0.44	0.98

Table S2. Comparison of Pseudocapacitor Performance Parameters of the CoZn-ZIF@MXene electrode with already Reported MOF Composite Electrodes.

S. no.	Electrode material	Specific capacitance (F/g)	Current density (A/g)	Refs.
1	ZIF-67@PCNFs40-300C	307.7	0.1	[5]
2	rGO/ZIF-67	210	1	[6]
3	ZIF-8@MWCNT-derived carbon	326	1	[7]
4	2-Ag@ZIF-8	538.8	1	[8]
5	nitrogen-doped porous carbon/CNT	324	0.5	[9]
6	MXene@CFT	474.23	1.5	[10]
7	CoZn-ZIF@MXene	622.95	1	This work

References

1. Y. Geng, S. Bi, J. Zhang, H. Li, G. Dai, Y. Zhang, Z. Xia, Q. Yang, G. Xie and S. Chen, *ACS Applied Nano Materials*, 2025, **8**, 5218-5228.
2. T.-E. Hsu, K. Manjunatha, M.-K. Ho, H.-H. Chiu, S.-L. Yu, B.-L. Lyu, Y.-T. Yu, H.-C. Kuo, S.-W. Yu and C.-L. Cheng, *ACS Applied Electronic Materials*, 2025, **7**, 3704-3724.
3. S. Jadhav, C. Ramana, S. Tan, S. Gosavi and S. Haram, *ACS Applied Energy Materials*, 2025, **8**, 1308-1321.
4. B. T. Al-Abawi, N. Parveen, S. A. Ansari, H. A. Al-Dosari, H. K. Alshaikh, A. Umar, A. A. Ibrahim and S. Akbar, *International Journal of Energy Research*, 2025, **2025**, 5331742.
5. T. Nakkhong, T. Inprasit and A. Pangon, *Chemical Engineering Journal*, 2024, **497**, 154655.

6. A. Hosseinian, A. Amjad, R. Hosseinzadeh-Khanmiri, E. Ghorbani-Kalhor, M. Babazadeh and E. Vessally, *Journal of Materials Science: Materials in Electronics*, 2017, **28**, 18040-18048.
7. Y. Wang, B. Chen, Y. Zhang, L. Fu, Y. Zhu, L. Zhang and Y. Wu, *Electrochimica Acta*, 2016, **213**, 260-269.
8. M. R. Karim, C.-H. Choi, A. Mohammad and T. Yoon, *Journal of Energy Storage*, 2024, **93**, 112199.
9. L. Wan, E. Shamsaei, C. D. Easton, D. Yu, Y. Liang, X. Chen, Z. Abbasi, A. Akbari, X. Zhang and H. Wang, *Carbon*, 2017, **121**, 330-336.
10. M. S. Javed, H. Lei, H. U. Shah, S. Asim, R. Raza and W. Mai, *Journal of Materials Chemistry A*, 2019, **7**, 24543-24556.